NANO LETTERS

Letter

pubs.acs.org/NanoLett

Biologically Tunable Reactivity of Energetic Nanomaterials Using Protein Cages

Joseph M. Slocik, Christopher A. Crouse, Jonathan E. Spowart, and Rajesh R. Naik*

Materials and Manufacturing Directorate, Air Force Research Lab, Wright-Patterson Air Force Base, Dayton, Ohio 45433-7750, United States

Supporting Information

ABSTRACT: The performance of aluminum nanomaterial based energetic formulations is dependent on the mass transport, diffusion distance, and stability of reactive components. Here we use a biologically inspired approach to direct the assembly of oxidizer loaded protein cages onto the surface of aluminum nanoparticles to improve reaction kinetics by reducing the diffusion distance between the reactants. Ferritin protein cages were loaded with ammonium perchlorate (AP) or iron oxide and assembled with nAl to create an oxidation−reduction based energetic reaction and the first demonstration of a nanoscale biobased thermite material. Both materials showed enhanced exothermic behavior in comparison to nanothermite mixtures of bulk free AP or synthesized iron oxide nanopowders prepared without the use of ferritin. In addition, by utilizing a layer-by-layer (LbL) process to build multiple layers of protein cages containing iron oxide and iron oxide/AP on nAl, stoichiometric conditions and energetic performance can be optimized.

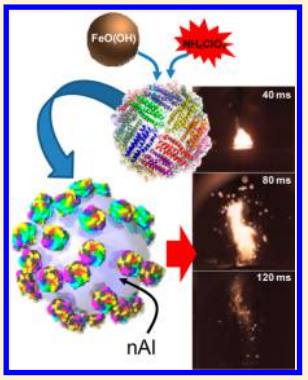

KEYWORDS: *Bioenergetics, ferritin, aluminum nanoparticles, thermite, protein cages*

Metals contain and release a large amount of stored energy due to their chemical composition and, as a result, are regularly used in propellants, explosives, and pyrotechnics.[1] Conventional formulations utilize micrometer-scale reactive metal powders (e.g., Al, Mg, Si) as fuel/additives to achieve/improve combustion efficiency and energy output.[2] Alternatively, aluminum metal prepared as a nanopowder (nAl) is of interest as an energetic material because of its superior properties and, more recently, enhanced processability.[3] It has a higher energy density than organic explosives and the potential for enhanced rates of reaction as compared to micrometer-sized Al powder due to a higher specific surface area. Additionally, nAl typically contains a thin oxide layer making it less pyrophoric and more amenable to functionalization and assembly with other reactive materials.[4−6] These features afford the opportunity to use nAl for nontraditional applications which could encompass microthrusters, new types of nanothermites, and explosive additives. Unfortunately, the energetic properties of current nAl based reactive systems are limited in part by the mass transport and diffusion distance between reactants/oxidizers, inhomogeneity and assembly of components, lack of well-defined interfaces, and instability of oxidizers.

Alternatively, biomolecules can be used in the precise control of ion transport, direct the synthesis and assembly of exquisitely structured nanomaterials, act as a storage reservoir for inorganic or genetic materials, and to exploit biomolecule−nanomaterial interactions.[9] The iron storage protein ferritin best exemplifies several of these functions packaged into a single biological nanostructure. Physiologically, ferritin is essential in regulating the molecular diffusion of Fe^{3+} ions into and out of the spherical protein cage, storing reservoirs of Fe^{3+} as hydrous ferric oxyhydroxide FeO(OH) nanoparticles within the hollow protein cavity, and then releasing Fe ions when needed.[7] Consequently, ferritin is well-established in materials science for its well-defined and stable protein structure, genetically and chemically addressable molecular components, and its ability to serve as a constrained biomimetic cage for nanoparticle synthesis.[8] We and others have genetically modified ferritin cages for the confined synthesis of monodisperse Au, Ag, CdS, Pd, TiO_2, Fe_3O_4, and UO_2 nanoparticles, molecular transport/storage of small molecules for drug delivery, and assembly on titania, carbon nanotube, and gold surfaces by addition of a metal-binding peptide on the exterior cage.[9−15] In these assemblies, the close proximity of ferritin to the nanomaterial surface resulted in enhanced optical and electrical properties.[16]

In this study, we used modified protein cages (ferritins) to tailor the energetic properties of aluminum nanoparticles (nAl) by modifying its surfaces with loaded ferritin cages. Ferritin cages loaded with iron oxide nanoparticles or ammonium perchlorate were assembled with nAl (Figure 1). By doing so, the diffusion distance is reduced between an encapsulated oxidizer within ferritin and the reactive nAl surface, leading to an increase in overall reaction kinetics and energy output. Notably, the assembly of biologically derived iron oxide loaded ferritin and nAl is chemically equivalent to a hermite (metal oxide plus a reactive metal) and represents, to the best of our knowledge, the first example of a biothermite material utilizing a natural system

Received: February 14, 2013
Revised: May 14, 2013
Published: May 28, 2013

dx.doi.org/10.1021/nl400590k | *Nano Lett.* 2013, 13, 2535−2540

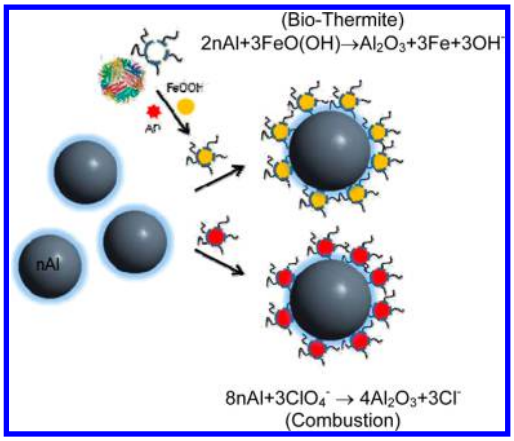

Figure 1. Assembly of nAl particles with cationized ferritin loaded with iron oxide or ammonium perchlorate. Energetic reactions of nAl with iron oxide or ammonium perchlorate are included as chemical equations. The ferritin structure is from Protein Data Bank (PDB 3H7g).

with properties and applications rivaling those of traditional thermites. In both cases, we observed increased exothermic behavior for the bioassembled hybrid systems as compared to the addition of bulk iron oxide or free ammonium perchlorate with nAl. Finally, we used a layer-by-layer (LbL) approach to control the reaction stoichiometry of nAl by tailoring the number of protein layers and ultimately tuning the energetic properties.

To determine the maximal binding interaction of the protein cage with nAl, we first tested different ferritin cages by binding to an aluminum oxide (alumina α-Al_2O_3) coated quartz crystal using a quartz crystal microbalance (QCM). The set consisted of a chemically modified ferritin cage with a positively charged surface (cationized ferritin), (apo)ferritin functionalized on its external surface with an aluminum binding peptide,[17] and an unmodified native ferritin with a carboxylate-rich surface. In total, each ferritin protein addressed the effects of surface chemistry and charge on nAl binding. By QCM, the cationized ferritin (zeta potential +23.6 ± 8.0 mV) showed the highest binding to the alumina substrate; while the unmodified native ferritin (zeta potential −32.9 ± 8.7 mV)[18] and apoferritin functionalized with an aluminum binding peptide showed minimal binding (Supporting Information, Figure S1). This difference is consistent with the favorable binding interaction of positively charged peptides or polymer ligands with negatively charged metal oxide surfaces.[19,20] As a result, we selected cationized ferritin from the protein set for assembly with nAl.

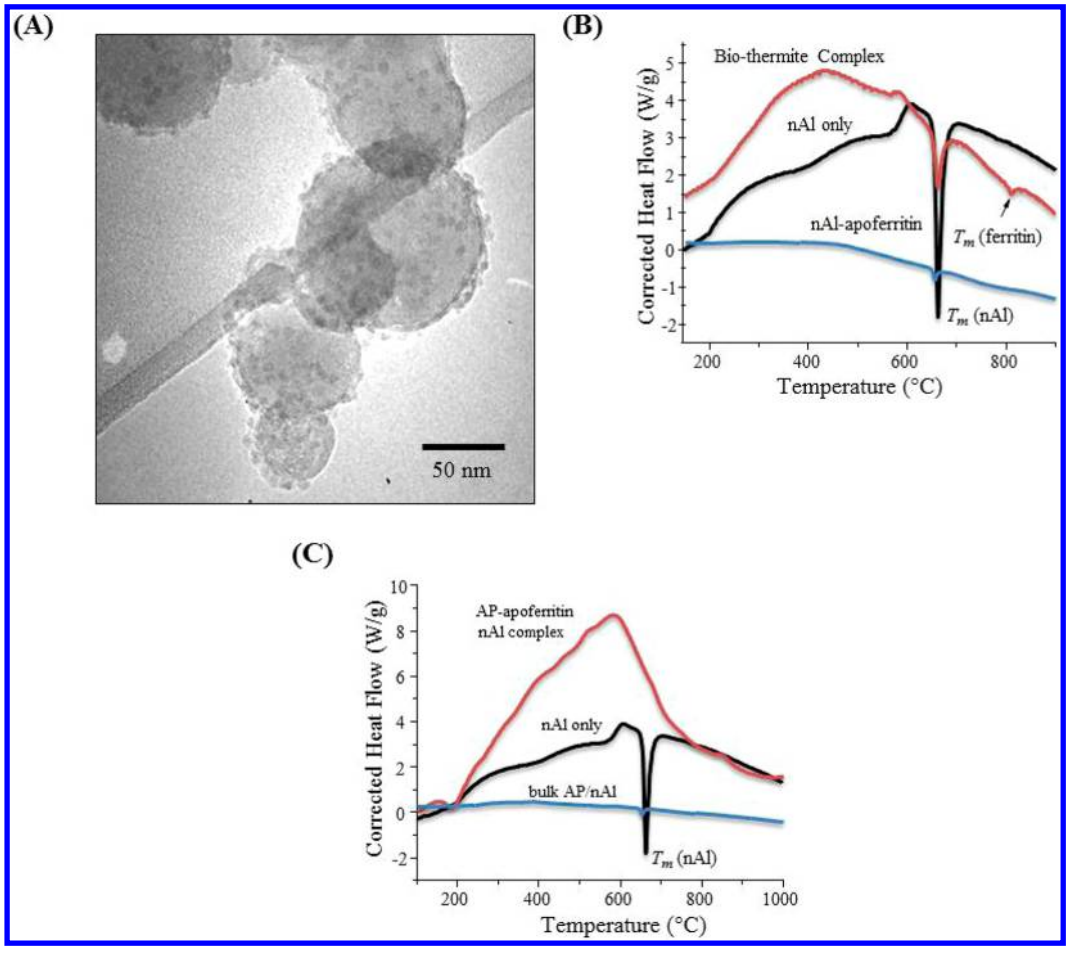

Figure 2. nAl assembled with iron oxide loaded cationized ferritin or AP loaded cationized apoferritin. (A) TEM micrograph showing nAl particle coated with cationized ferritin. (B) TGA/DTA profile of nAl assembled with one-layer of iron oxide loaded cationized ferritin, unfunctionalized nAl, and nAl assembled with two-layers of apoferritin (no iron oxide). (C) TGA/DTA profile of AP loaded cationized apoferritin/nAl at maximal loading of AP, unfunctionalized nAl, and nAl + bulk AP. For bulk AP reaction, 30 wt % AP is mixed with unfunctionalized nAl to yield an equivalency ratio f of 3.2 that is near stoichiometric conditions (ϕ = 1).

dx.doi.org/10.1021/nl400590k | *Nano Lett.* 2013, 13, 2535−2540

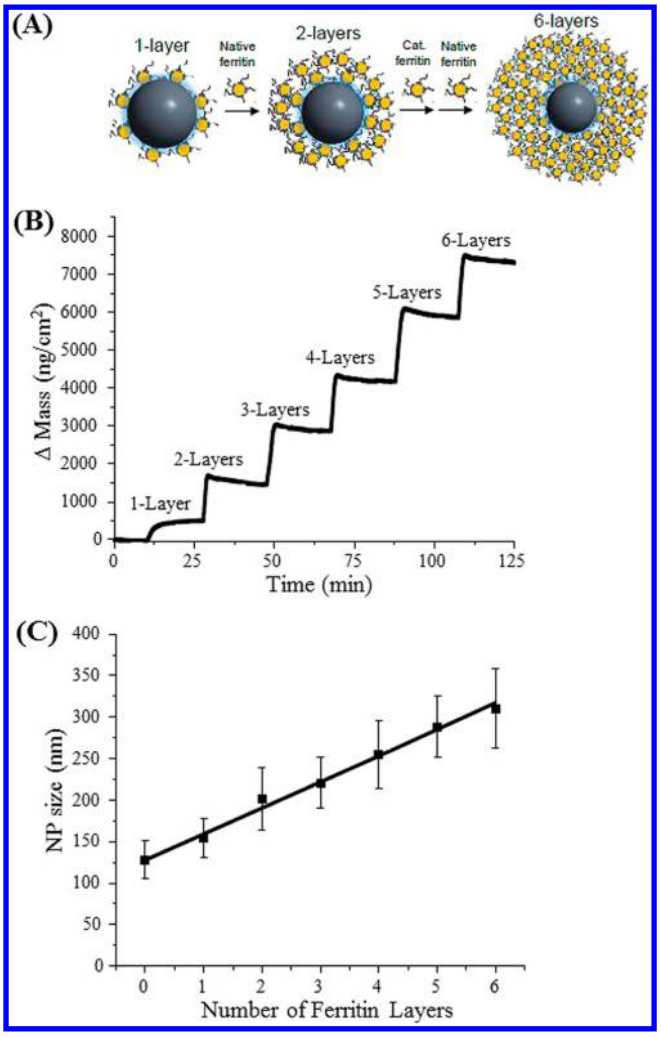

Figure 3. (A) Layer-by-layer assembly of cationized ferritin and negatively charged ferritin on nAl. (B) Quartz crystal microbalance plot showing layer-by-layer assembly of cationized ferritin and native ferritin on an aluminum oxide coated QCM substrate. Frequency is plotted at 3rd overtone and measured at a flow rate of 0.17 mL/min. (C) Plot showing the size of ferritin/nAl complex with increasing layers of protein cages using dynamic light scattering.

Cationized ferritin protein cages filled with an iron oxide core were assembled with 80 nm nAl particles. When visualized by TEM, the nAl particles were found to be uniformly decorated with iron oxide loaded cationized ferritin cages (Figure 2A). Each ferritin cage contains an iron oxide particle that is ~6 nm in diameter and in the biologically active form of ferrihydrite, FeO(OH), as depicted by the dark electron dense cores on the surface of nAl in the TEM micrograph. The assembled structure yielded a wt % ratio of 10.7 nAl to 1.0 Fe and an equivalency ratio of 31.7 [equivalency ratio ϕ = $(\text{fuel/oxidizer})_{\text{actual}}/(\text{fuel/oxidizer})_{\text{stoichiometric}}$] as measured by energy dispersive X-ray analysis (EDAX). In contrast, the assembly of nAl with native ferritin (negatively charged) resulted in a few protein cages associated with the nAl surface by TEM and no detectable Fe by EDAX (Supporting Information, Figure S2). Initial measurements of the energetic performance of the biothermite materials were obtained by simultaneous thermogravimetric analysis (TGA) and differential thermal analysis (DTA) under an argon environment to prevent oxidation. As a baseline, the TGA/DTA profile of unfunctionalized nAl particles showed a broad exotherm occurring between 100 and 350 °C due to the conversion of amorphous-Al_2O_3 to γ-Al_2O_3 and a sharp endothermic peak at 660 °C from the melting of nAl (Figure 2B).[6] The mild exothermic properties occur from the slow diffusion of trace amounts of oxygen present in the argon gas and limited reaction with nAl. The characteristic melting peak of nAl provides a means to assess how much aluminum is consumed during the course of the reaction and whether or not stoichiometric conditions are reached. Also, when nAl was assembled with two layers of apoferritin (empty no iron oxide), we observed no exotherm. We attribute this lack of an exotherm to the formation of a carbide layer on aluminum that acts as a gas impermeable barrier. Alternatively, when cationized ferritin was mixed with the nAl powder, the exotherm appeared prior to aluminum melting with a reaction onset at 300 °C and was greater than the unfunctionalized nAl/two-layer apoferritin-nAl complex. Additionally, we observed a decreased aluminum melting peak due to consumption of nAl with the cationized ferritin and a small endothermic peak at ~800 °C which is also present in the TGA/DTA profile of ferritin by itself and attributed to a phase transition of ferrihydrite FeO(OH) to magnetite (Fe_3O_4) (Supporting Information, Figure S3).

In addition to using the biologically synthesized iron oxide core of ferritin to create biothermite materials, we loaded cationized apoferritin cages with ammonium perchlorate (NH_4ClO_4; AP) to increase combustion kinetics of nAl through an oxidation reaction. AP is a strong oxidizer which decomposes at low temperatures (<200 °C) and releases energy when mixed with reactive metals such as nAl.[21] We first removed the ferrihydrite mineral core from inside the ferritin protein cage by reductive dissolution with 0.5% mercaptoacetic acid in 0.1 M acetate buffer pH 4.5 and repeated dialysis.[22] The empty cage (apoferritin) as determined by UV−vis spectroscopy and high resolution XPS (Supporting Information, Figure S4) was then subsequently filled via successive additions of 0.1 M AP or a rhodamine perchlorate analogue and followed by multiple dialysis steps to obtain maximal loading. In this approach, the 3-fold hydrophilic pores of ferritin allow molecular transport of AP into the internal cavity where it accumulates and balances the interior charges.[23] Initially, rhodamine perchlorate was used to spectroscopically show incorporation and diffusion into the cage by coelution of loaded apoferritin on a size exclusion chromatography column (Supporting Information, Figure S5). Upon AP loading and assembly with nAl, XPS confirmed the presence of 0.6% Cl, 0.8% N, and 8.9 atomic % of Al (Supporting Information, Figure S6). This is equivalent to a stoichiometry of ~2800 AP molecules/protein cage and suggests that AP fills the interior protein cavity rather than only interacting with the positive charges on the exterior protein surface. In this latter case, we would expect to obtain a maximum of ~170 AP molecules given the presence of 170 net positive charges on cationized apoferritin if there were only surface interactions. Energetically, the TGA/DTA profile of AP loaded ferritin-nAl showed much greater exothermic behavior as compared to the biothermite sample (Figure 2C). For this material, the entire event was exothermic using only a single layer of cationized apoferritin molecules filled with AP (ϕ = 27.1). By comparison, the addition of much higher quantities of free AP at 30 wt % (ϕ = 3.2) recrystallized with nAl resulted in the thermal decomposition of AP below 200 °C and a flat profile by TGA/DTA (Figure 2C).[24] Importantly, this confirms the thermal stabilization of AP upon entrapment by the ferritin protein cage and its critical role in reacting with nAl under fuel-rich conditions.

dx.doi.org/10.1021/nl400590k | Nano Lett. 2013, 13, 2535−2540

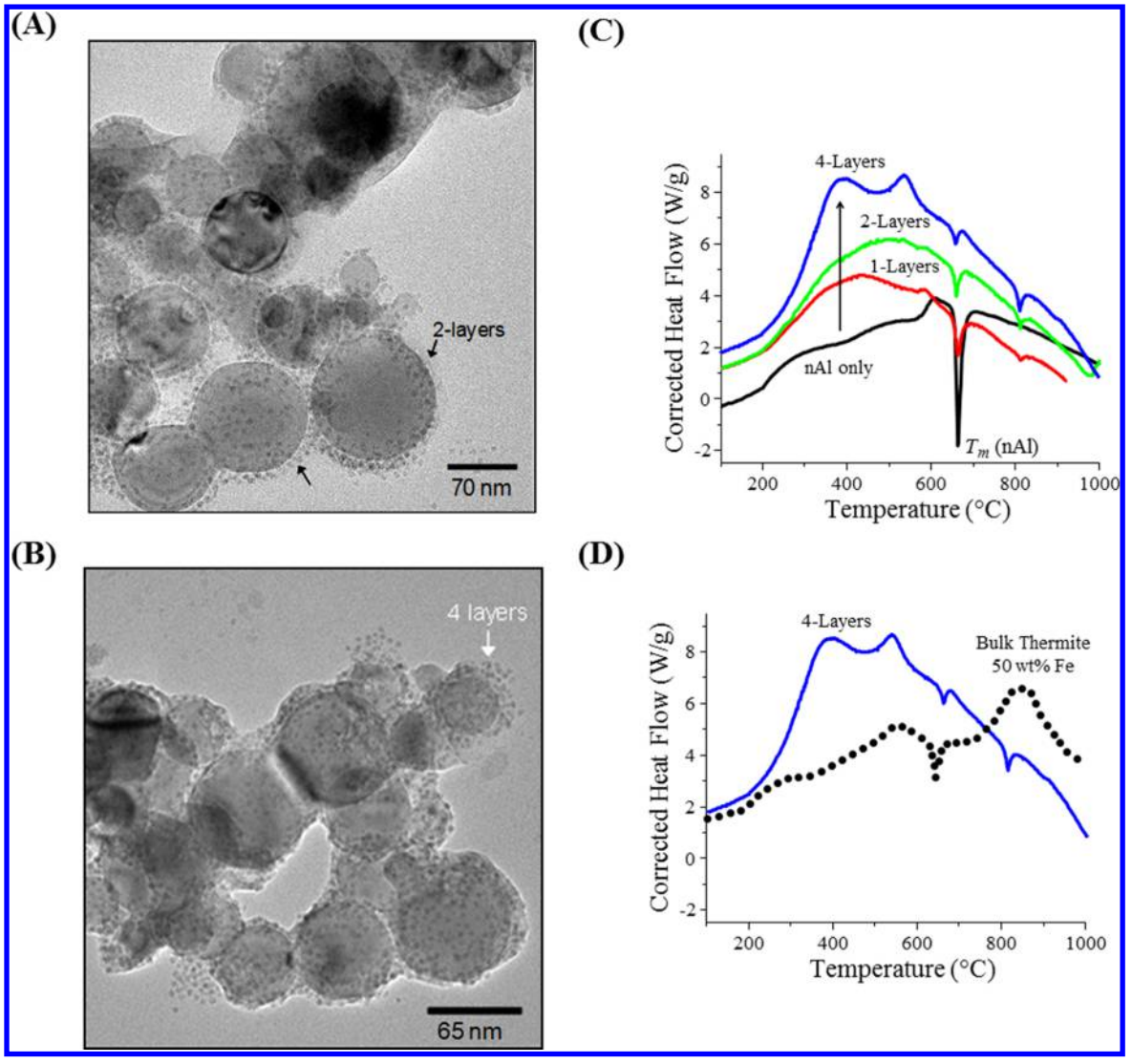

Figure 4. TEM micrographs and energetic properties of nAl coated by multi-layers of FeO(OH) loaded ferritin. (A) Two-layer ferritin on nAl. (B) Four-layer ferritin on nAl. (C) DTA heat profile for two-four layers of iron oxide loaded ferritin with nAl. The heat profile for unfunctionalized nAl is also included. (D) DTA heat profile for nAl coated with four-layer iron oxide loaded ferritin and a bulk thermite reaction composed of micron sized Fe_2O_3 powder with nAl at 50:50 wt % (equivalency ratio = 2.9).

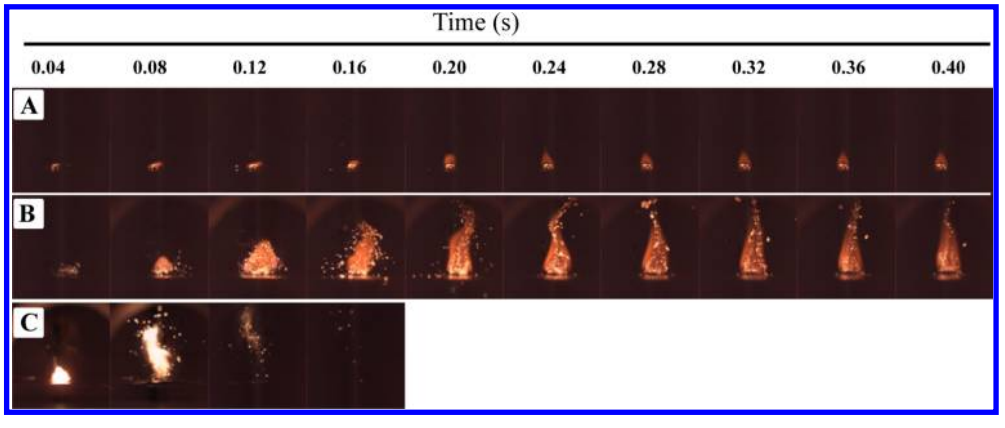

Figure 5. Visualization of combustion of ferritin/nAl materials at selected time frames using high speed camera. (A) Two-layer apoferritin-nAl with no FeO(OH). (B) Two-layer ferritin/FeO(OH)-nAl. (C) One-layer AP loaded cationized apoferritin/nAl.

Given the promising exothermic properties of the single layer AP loaded cationized apoferritin/nAl and biothermite systems, we used a layer-by-layer (LbL) process to create hybrid particles with greater reactivity by coating nAl with multiple layers of ferritin cages bearing iron oxide particles. According to the chemical reactions shown in Figure 1, the biothermite reaction

dx.doi.org/10.1021/nl400590k | *Nano Lett.* 2013, 13, 2535−2540

requires more FeO(OH) to reach balanced stoichiometric conditions which are slightly fuel-rich. To achieve higher iron oxide loading with nAl and achieve stoichiometric conditions (ϕ = 1), we alternated the addition of native ferritin with cationized ferritin to build additional protein layers and reach the desired wt % as confirmed by QCM and dynamic light scattering (DLS) (Figure 3). Previous BioLbL processes have been used to form silk LbL microcapsules,[25] free-standing polyelectrolyte redox films of polytyrosine,[26,27] and composite layers of titania with peptide modified ferritin.[28] In our LbL assembled structures, alternating layers of negatively charged native ferritin and cationized ferritin with zeta potentials of −32.9 ± 8.7 mV and +23.6 ± 8.0 mV, respectively, were electrostatically assembled around nAl. QCM showed the formation of multiple layers of iron oxide loaded ferritins of equal mass on an aluminum oxide coated QCM sensor (Figure 3B), while DLS analysis showed a linear increase in the hydrodynamic radius of nAl particles upon sequential addition of protein layers (Figure 3C). By TEM, alternating layers of cationized and native ferritin loaded only with iron oxide was observed around the surface of nAl in uniformly spaced layers (Figure 4A,B, Supporting Information Figure S7). In total, we have assembled as many as 12 layers of iron oxide loaded ferritin around nAl with good coverage. Energetically, the corresponding DTA profile of the multilayer ferritin decorated nAl particles showed increasing exotherms as the number of layers increased from 1 to 4 and higher consumption of nAl as observed by a decreased melting nAl peak (Figure 4C), while TGA showed increasing weight loss (Supporting Information, Figure S8). The magnitude of the exotherm was dependent upon the weight ratio of nAl to iron oxide loaded ferritin, whereby slightly fuel rich mixtures comprised of four layers (ϕ = 5.5) produced the largest exotherm (Supporting Information, Figure S9). For comparison, we measured the heat profile generated from a bulk thermite reaction of micrometer sized iron oxide particles and nAl particles at 50 wt % (ϕ = 2.9) (Figure 4D). In this thermite reaction, the exotherm was not observed until 750−950 °C, and it released a lower amount of heat at a smaller equivalency ratio. Consequently, the biothermite reaction yielded larger exotherms at a lower temperature range, while also consuming more of the aluminum at near stoichiometric conditions. This onset of combustion at lower temperatures is due to the high surface area of nAl, reduced melting point, shorter diffusion distance, and possible cooling effects from gasification of the ferritin protein cage. Consequently, these lower ignition temperatures are preferred for certain applications since less activation energy is required to initiate the self-sustaining combustion reaction which results in more complete combustion, faster reaction kinetics, and an overall higher energy.

Additionally, we analyzed and compared the combustion characteristics of our protein assembled nAl materials using a high speed camera. Unlike TGA/DTA, this burn test provides a means to qualitatively test the energetic behavior, performance, and reaction kinetics of each material in a real world scenario and under normal combustion conditions. The materials were ignited using a flame from a butane torch, recorded using a color high speed digital video camera during the course of combustion, and analyzed at individual time frames. As a control, we first ignited a two-layer apoferritin coated nAl sample with no FeO(OH) (Figure 5A). From the high speed video, the two-layer apoferritin-nAl powder burned slowly, yielding only a faint glow. This minimal combustion was limited by the slow diffusion and reaction with atmospheric oxygen. However, upon addition of iron oxide to form the two-layer loaded ferritin structure, we observed a much greater combustion event (Figure 5B). This combustion event featured a large intense flame and the appearance of several sparks generated due to the flocculant nature of the electrostatically charged powder. When we increased the amount of iron oxide loaded ferritins to 12 layers on nAl, we obtained an even a larger flame which burned much faster (Supporting Information, Figure S10). By comparison, more iron oxide was consumed, leading to faster combustion rates and a release of more energy. This supports the enhanced role of multiple protein layers on reaction kinetics and confirms that transport properties are not sacrificed when as many as 12 layers are assembled on nAl due to its high surface area. In these materials, the ferritin protein cages also provide an abundant source of carbon, nitrogen, and oxygen in the form of amino acids (∼15 wt % of protein in a two-layer structure) which likely promotes increased gas production, higher pressures, and faster flame speeds during the initial combustion process which is greatly desired for propellant applications. Conversely, upon substitution of the iron oxide for the stronger oxidizing agent AP in cationized apoferritin, we observed an impressive combustion of the single layer AP loaded material (Figure 5C). The nAl was rapidly consumed upon reacting with the encapsulated AP, and the reaction was essentially complete after 160 ms.

Using a protein cage to enable the assembly of inorganic or oxidizing agents, we achieved enhanced reaction rates and increased energy output of nAl materials as demonstrated by the assembly of biothermites and AP loaded protein-nAl systems. The protein cages offer the ability to encapsulate/stabilize an inorganic material or oxidizing agent and interact/coat the surface of reactive nanomaterials, thereby quickly delivering these materials to the reactive nAl surface by reducing the diffusion distance and mass transport of reactants and providing a source of carbon and nitrogen to increase combustion pressures. Also, we were able to control the reaction stoichiometry of nAl with iron oxide or AP by utilizing more or fewer protein layers and ultimately tailor the energetic properties. Potentially, each protein layer can be customized with an inorganic material, molecular explosive, and/or oxidizing agent on demand depending on the desired application. For example, we envision additional gains in energetic properties by substitution of the ferrihydrite FeO(OH) core of ferritin with different crystalline phases of iron oxide (Fe_2O_3 and Fe_3O_4) and/or the use of larger protein cages such as viral capsids (100 nm in size) to accommodate larger sized iron oxide particles or molecular cargo. Using a bioderived route also provides the opportunity for the development of safer and more efficient combustible materials. Ultimately, we can extend this approach to the design of nonbiological routes, that is, LbL, to make hybrid combustible materials.

■ ASSOCIATED CONTENT

Supporting Information

Materials and methods; supporting figures. This material is available free of charge via the Internet at http://pubs.acs.org.

■ AUTHOR INFORMATION

Corresponding Author

*E-mail: Rajesh.Naik@wpafb.af.mil.

Notes

The authors declare no competing financial interest.

■ ACKNOWLEDGMENTS

This work was funded by the Air Force Office of Scientific Research. We thank Dr. Patrick Dennis for helpful discussions and providing the ferritin protein functionalized with aluminum-binding peptides and Dr. Steve Kim for providing nAl-ferritin graphic for the TOC figure.

■ REFERENCES

(1) Yen, N. H.; Wang, L. Y. *Propellants, Explosives, Pyrotechnics* **2012**, *37*, 143−155.
(2) Dreizin, E. L. *Prog. Energy Combust.* **2009**, *141*, 35.
(3) Yarrington, C. D.; Son, S. F.; Foley, T. J.; Obrey, S. J.; Pacheco, A. N. *Propellants, Explosives, Pyrotechnics* **2011**, *36*, 551−557.
(4) Crouse, C. A.; Pierce, C. J.; Spowart, J. E. *ACS Appl. Mater. Interfaces* **2010**, *2*, 2560−2569.
(5) Nixon, E.; Pantoya, M. L.; Sivakumar, G.; Vijayasai, A.; Dallas, T. *Surf. Coat. Technol.* **2011**, *205*, 21−22.
(6) Watson, K. W.; Pantoya, M. L.; Levitas, V. I. *Combust. Flame* **2008**, *155*, 619−634.
(7) Chasteen, N. D.; Harrison, P. M. *J. Struct. Biol.* **1999**, *126*, 182−194.
(8) Masaki, U.; Klem, M. T.; Allen, M.; Suci, P.; Flenniken, M.; Gillitzer, E.; Varpness, Z.; Liepold, L. O.; Young, M.; Douglas, T. *Adv. Mater.* **2007**, *19*, 1025−1042.
(9) Dickerson, M. B.; Sandhage, K. H.; Naik, R. R. *Chem. Rev.* **2008**, *108*, 4935−4978.
(10) Kramer, R. M.; Li, C.; Carter, D. C.; Stone, M. O.; Naik, R. R. *J. Am. Chem. Soc.* **2004**, *126*, 13282−13286.
(11) Sano, K. I.; Shiba, K. *MRS Bull.* **2008**, *33*, 524−529.
(12) Kobayashi, M.; Kumagai, S.; Zheng, B.; Uraoka, Y.; Douglas, T.; Yamashita, I. *Chem. Commun.* **2011**, *47*, 3475−3477.
(13) Zheng, B.; Zettsu, N.; Fukuta, M.; Uenuma, M.; Hashimoto, T.; Gamo, K.; Uraoka, Y.; Yamashita, I.; Watanabe, Y. *Chem. Phys. Lett.* **2011**, *1−3*, 76−80.
(14) Caruso, F.; Furlong, D. N.; Kingshott, P. *J. Colloid Interface Sci.* **1997**, *186*, 129−140.
(15) Fan, R.; Chew, S. W.; Cheong, V. V.; Orner, B. P. *Small* **2010**, *6*, 1483−1487.
(16) Briggs, B. D.; Knecht, M. R. *J. Phys. Chem. Lett.* **2012**, *3*, 405−418.
(17) Zuo, R. J.; Ornek, D.; Wood, T. K. *Appl. Microbiol. Biotechnol.* **2005**, *68*, 505−509.
(18) Sengonul, M.; Ruzicka, J.; Attygalle, A. B.; Libera, M. *Polymer* **2007**, *48*, 3632−3640.
(19) Vallee, A.; Humblot, V.; Pradier, C.-M. *Acc. Chem. Res.* **2010**, *43*, 1279−1306.
(20) Chen, C.-L.; Rosi, N. L. *Angew. Chem., Int. Ed.* **2010**, *49*, 1924−1942.
(21) Stephens, M.; Sammet, T.; Peterson, E.; Carro, R.; Wolf, S.; Smith, C. *J. Prop. Power* **2010**, *26*, 461−466.
(22) Wong, K. K. W.; Douglas, T.; Gider, S.; Awschalom, D. D.; Mann, S. *Chem. Mater.* **1998**, *10*, 279−285.
(23) Douglas, T.; Ripoll, D. R. *Protein Sci.* **1998**, *7*, 1083−1091.
(24) Li, S. F.; Jiang, Z.; Zhao, F. Q.; Liu, Z. R.; Yin, C. M.; Luo, Y.; Li, S. W. *Chin. J. Chem. Phys.* **2004**, *17*, 623−628.
(25) Shchepelina, O.; Drachuk, I.; Gupta, M. K.; Lin, J.; Tsukruk, V. V. *Adv. Mater.* **2011**, *23*, 4655.
(26) Kharlampieva, E.; Slocik, J. M.; Tsukruk, T.; Naik, R. R.; Tsukruk, V. V. *Chem. Mater.* **2008**, *20*, 5822−5831.
(27) Jan, J. S.; Chen, P. J.; Ho, Y. H. *J. Colloid Interface Sci.* **2011**, 358.
(28) Sano, K.; Sasaki, H.; Shiba, K. *J. Am. Chem. Soc.* **2006**, *128*, 1717−1722.